



# A bioinformatics-based immune-related prognostic index for lung adenocarcinoma that predicts patient response to immunotherapy and common treatments

Chenghao Wang<sup>1#^</sup>, Tong Lu<sup>1#</sup>, Ran Xu<sup>1</sup>, Xiaoyan Chang<sup>1</sup>, Shan Luo<sup>2</sup>, Bo Peng<sup>1</sup>, Jun Wang<sup>1</sup>, Lingqi Yao<sup>1</sup>, Kaiyu Wang<sup>1</sup>, Zhiping Shen<sup>1</sup>, Jiaying Zhao<sup>1</sup>, Linyou Zhang<sup>1</sup>

<sup>1</sup>Department of Thoracic Surgery, The Second Affiliated Hospital of Harbin Medical University, Harbin, China; <sup>2</sup>Second Clinical College of Medicine, Harbin Medical University, Harbin, China

**Contributions:** (I) Conception and design: L Zhang, J Zhao; (II) Administrative support: T Lu, R Xu; (III) Provision of study materials or patients: B Peng, K Wang, Z Shen; (IV) Collection and assembly of data: S Luo, J Wang, L Yao; (V) Data analysis and interpretation: C Wang, X Chang; (VI) Manuscript writing: All authors; (VII) Final approval of manuscript: All authors.

<sup>#</sup>These authors contributed equally to this work.

**Correspondence to:** Jiaying Zhao; Linyou Zhang. Department of Thoracic Surgery, The Second Affiliated Hospital of Harbin Medical University, Harbin, China. Email: Jiayingz8912@126.com; lyzhang@hrbmu.edu.cn.

**Background:** There is increasing evidence of the effectiveness of immune checkpoint blockade (ICB) therapy for the treatment of lung adenocarcinoma (LUAD). However, the benefits of ICB therapy vary among LUAD patients. Due to the research dimension, existing biomarkers, such as programmed death-ligand 1 (PD-L1) expression and tumor mutation burden (TMB), could not reflect the complex tumor environment, and had low prediction accuracy of ICB. Therefore, we aimed to uncover a prognostic biomarker that could also predict whether a patient would benefit from ICB therapy and other common treatments from multiple dimensions, so as to improve the prediction accuracy of pre-treatment patients.

**Methods:** Based on the LUAD dataset retrieved from The Cancer Genome Atlas (TCGA) database, 50 immune-related hub genes were identified using weighted gene co-expression network analysis and univariate Cox regression analyses. An immune-related gene prognostic index (IRGPI) was constructed using a Cox proportional-hazards model based on 15 genes and validated using GSE72094 dataset. We tested its prognostic accuracy by Kaplan-Meier (K-M) survival curves of the two datasets and assessed its predictive power by comparing area under curve (AUC) of IRGPI with existing biomarkers. Subsequently, we analyzed the molecular and immune characteristics, and evaluated the benefits of ICB by PD-L1 expression and Tumor Immune Dysfunction and Exclusion (TIDE) analysis, predicted the inhibitory concentration 50 of common treatments drugs for two IRGPI score-related subgroups.

**Results:** Patients in the IRGPI-high subgroup had lower overall survival (OS) than patients in the IRGPI-low subgroup in K-M survival curve in two cohorts. And IRGPI has AUC values of 0.715, 0.724, and 0.743 in 1, 2, and 3 years, respectively. A higher tumor mutation burden and PD-L1 expression and the tumor microenvironment (TME) landscape demonstrated that IRGPI-high subgroup patients may respond better to ICB therapy. Genomics of Drug Sensitivity in Cancer (GDSC) analysis indicated that the IRGPI-high subgroup showed greater sensitivity to chemotherapy.

**Conclusions:** IRGPI is a prospective biomarker for evaluating whether a patient will benefit from ICB therapy and other treatments, and distinguishing patients with different molecular and immune characteristics.

**Keywords:** Immune-related genes; immune checkpoint blockade therapy (ICB therapy); lung adenocarcinoma (LUAD); prognosis biomarker; immune cell infiltration

<sup>^</sup> ORCID: 0000-0002-2024-8156.

Submitted Mar 22, 2022. Accepted for publication May 27, 2022.

doi: 10.21037/jtd-22-494

View this article at: <https://dx.doi.org/10.21037/jtd-22-494>

## Introduction

Lung cancer is one of the leading causes of cancer deaths worldwide, with 2.35 million new cases and 1.31 million deaths in the United States in 2021 alone (1). This disease is histologically divided into 2 categories, small cell lung cancer (SCLC) and non-small cell lung cancer (NSCLC). Within NSCLC, the major histological subtype, lung adenocarcinoma (LUAD) accounts for 40% of cases (2). Treating lung cancer involves a combination of surgical resection, chemotherapy, radiotherapy, and immunotherapy (3). Chemotherapy and molecular-targeted therapy are 2 common treatment strategies used for LUAD, while first-line treatment for patients with advanced LUAD is platinum-based combination chemotherapy (4). Immune checkpoint blockade (ICB) therapy is now an alternative option to treat LUAD (5). However, multiple factors, including the tumor microenvironment (TME), influence ICB therapy. The cellular heterogeneity of cancer cells and the TME contribute to disease progression and treatment resistance (6).

ICB therapy is an emerging anticancer weapon targeting T-cell regulatory pathways to enhance antitumor immune responses. Rather than activating the immune system to attack specific targets on tumor cells, this therapy aims to remove inhibitory pathways that block effective antitumor T-cell responses (7-9). ICB therapy has been shown to produce clinical responses in patients with a variety of tumor types (10). More specifically, anti-programmed death-ligand 1 (PD-L1) antibodies cause tumor regression in patients with different tumors, including NSCLC. Although ICB therapy shows significant clinical success, its efficacy varies widely among patients, especially NSCLC patients (11-15). However, existing biomarkers such as PD-L1 expression, TMB, etc. only reflect a small part of the tumor's response to immunotherapy from a single perspective such as ligand expression and gene mutation, do not fully reflect the interaction of different factors in the complex TME, and are limited in prediction.

In this study, from the perspective of immunity, we hope to establish an indicator: immune-related gene prognostic index (IRGPI) that can better predict therapeutic efficacy than existing biomarkers through immune-related genes.

At the same time, the different immune functions of genes in the model also more broadly reflect the important role of the immune system in tumor progression. Interestingly, in our analysis, the molecular and immunological characteristics of different IRGPI score-related subgroups were also quite different, which endows IRGPI with the ability to distinguish disease characteristics of LUAD patients. Our results suggested that IRGPI is an excellent prognostic index and has considerable advantages in predicting benefits of various treatments and distinguishing disease features for LUAD patients. We present the following article in accordance with the TRIPOD reporting checklist (available at <https://jtd.amegroups.com/article/view/10.21037/jtd-22-494/rc>).

## Methods

### *Gene expression datasets and study design*

RNA-sequencing data for 594 LUAD cases (59 normal tissues and 535 LUAD samples) and clinical and simple nucleotide variation (varscan2) data for 486 samples were downloaded from The Cancer Genome Atlas (TCGA) database (<https://portal.gdc.cancer.gov/>). Microarray data for 442 LUAD samples and survival data [Gene Expression Omnibus (GEO): GSE72094] were downloaded from the GEO database (<https://www.ncbi.nlm.nih.gov/geo/>). A list of immune genes was derived from the InnateDB (<https://www.innatedb.com/>) and the Immunology Database and Analysis Portal System (ImmPort) (<https://www.immport.org/shared/home>) databases. LUAD tumor samples downloaded from TCGA were divided into 6 immune subtypes based on 5 immune expression characteristics as previously described (16).

In this study, we first screened immune genes through differential expression analysis and weighted gene co-expression network analysis (WGCNA) analysis to obtain immune-related hub genes associated with LUAD. Using univariate and multivariate cox analyses, we built and tested a prognostic model and explored the molecular and immune characteristics of the two subgroups of the model. Finally, we tested the capability of the model to predict the patient's response to ICB therapy through PD-L1 expression,

Tumor Immune Dysfunction and Exclusion (TIDE), and other analyses. We also examined the sensitivity of different subgroups of the model to common treatments through Genomics of Drug Sensitivity in Cancer (GDSC) analysis. The study was conducted in accordance with the Declaration of Helsinki (as revised in 2013).

### *Immune-related hub genes*

Using the “limma” package in R (17), we performed differential expression analysis of RNA-seq FPKM (fragments per kilobase of exon per million mapped fragments) in LUAD samples downloaded from TCGA to obtain differentially expressed genes [DEGs; absolute values of log fold change (FC) >1 and false discovery rate (FDR) adjusted  $P < 0.05$ ]. After comparing the DEGs and the list of immune-related genes, the “clusterProfiler” package in R (18) was used to perform Gene Ontology (GO) analysis and Kyoto Encyclopedia of Genes and Genomes (KEGG) analysis on differentially expressed immune-related genes.

WGCNA was performed for the analyzed genes to obtain co-expression modules using the “WGCNA” package in R (19). First, the Pearson correlation coefficient for any 2 genes was calculated and a similarity matrix was established. The optimal soft threshold power,  $\beta = 4$ , was then obtained using unary linear regression, and the similarity matrix was transformed into an adjacency matrix based on the optimal soft threshold power before transforming it into a topological overlap matrix (TOM) to measure the correlation between 2 genes. After obtaining TOM, we clustered genes with 1-Tom set as the distance. Finally, by setting the minimum number of genes in each module to 25 and merging the threshold function of 0.25, we obtained clustering results. Three nongray modules (the blue, brown, and turquoise modules) were obtained, and the correlation of co-expression modules and traits (for both normal and tumor samples) were generated. We concluded that the absolute value for the turquoise module was the largest, and we constructed the network based on this.

A total of 50 immune-related hub genes significantly correlated ( $P < 0.05$ ) with the overall survival (OS) of LUAD patients, as shown by univariate Cox regression analysis of the 263 genes in the turquoise module. The “Survminer” package in R was used to calculate the optimal cut-off value for the expression of each gene. Based on the cut-off value, patients were divided into a high expression group and a low expression group. P values were calculated using the Kaplan-Meier (K-M) method and survival curves were

plotted. The “Maftools” package in R (20) was then used to analyze 50 hub gene-related mutation information obtained for the LUAD patients.

### *Construction of IRGPI*

To further screen genes that had a significant impact on patient prognosis, we conducted multivariate Cox regression analysis on immune-related hub genes and set the direction as ‘both’ to screen variables to obtain IRGPI. IRGPI, a Cox proportional-hazards model, was obtained by multiplying the expression values of specific genes by their coefficients. Based on the median value of IRGPI scores in the TCGA cohort, the cut-off point between IRGPI-high and IRGPI-low subgroups was obtained. The K-M method was used to perform survival analysis (log-rank test) for the TCGA and GEO cohorts to validate IRGPI values in predicting LUAD patient prognosis. Eventually, univariate and multivariate Cox regression analyses were performed for both IRGPI and common clinical factors, with the goal of further evaluating the independent prognostic ability of IRGPI.

### *Molecular and immune characteristics in 2 IRGPI subgroups*

To obtain the differentially expressed signal pathways for the 2 IRGPI subgroups, we used the “limma” package in R to conduct differential expression analysis of the subgroups based on TCGA expression data to obtain their DEGs. Subsequently, the “clusterProfiler” package in R was used to generate gene set enriched analysis (GSEA) based on GO and KEGG gene sets downloaded from the MsigDB database (<http://www.gsea-msigdb.org/>). We then used the “Maftools” package in R to analyze the simple nucleotide variation data of LUAD patients and to obtain genetic mutation information for the 2 subgroups. Difference analysis was performed for PD-L1 expression and tumor mutation burden (TMB) for both subgroups using the “limma” package in R.

The CIBERSORT online tool (<https://cibersort.stanford.edu/>) was used to study immune cell infiltration of 22 unique immune cells using 1,000 iterations in each sample. With this, the TME landscape of IRGPI was obtained. We then compared immune cell infiltration with clinicopathological factors for both subgroups. Subsequently, we used the “limma” package in R to analyze differences in the proportions of the 22 different immune cells in the IRGPI subgroups and plotted K-M survival

curves for immune cells showing significantly different proportions to determine which cells affected prognosis. To further explore the impact of immune-related function pathways on the prognosis of the subgroups, a single sample GSEA (ssGSEA) was performed using the “GSVA” package in R (21). Differential analysis was performed using the “limma” package in R and K-M survival curves were plotted for immune-related function pathways showing significant differences between the 2 subgroups.

To understand the association between immune and clinical grouping methods, we analyzed the distribution of immune subtypes and clinical stages for the different IRGPI subgroups using a chi-square test.

### *Prognostic ability, immune therapy response, and drug susceptibility of IRGPI*

To evaluate the predicted efficacy of immunotherapy in the different IRGPI subgroups, we downloaded the TIDE score online calculator (<http://tide.dfci.harvard.edu/>). The differences in TIDE, microsatellite instability (MSI), T-cell dysfunction, and T-cell exclusion scores of the 2 groups were analyzed using the “limma” package in R. To confirm the reliability of IRGPI as a prognostic biomarker, the “timeROC” package in R was used to perform time-dependent receiver operating characteristic (ROC) curve analysis for IRGPI, TIDE, and tumor inflammation signature (TIS). The areas under the curve (AUC) for each of these variables were generated and multiple time comparisons were performed.

Finally, we compared the half-maximal inhibitory concentration (IC<sub>50</sub>) of chemotherapy and targeted drugs for the treatment of LUAD for the 2 IRGPI subgroups using the GDSC online tool (<https://www.cancerRxgene.org/>) to obtain drug sensitivity information.

### *Statistical analysis*

R software (version 4.1.1) (<http://www.r-project.org/>) and its corresponding R packages were used for all statistical data analysis and to generate graphs. Using the “clusterProfiler” package in R, we completed GO, KEGG, and GSEA analyses. Time-dependent ROC curve plotting and AUC calculations were performed using the “timeROC” package in R.

The chi-square test was used to determine whether differences in other groupings of IRGPI were significant between the 2 groups. A log-rank test was used to draw

and compare K-M survival curves for univariate survival analysis. The Cox regression model was used to identify associated factors of survival outcomes. The AUC value of ROC curve greater than 0.7 is generally considered to be an excellent predictive model. P values less than 0.05 were considered statistically significant.

## **Results**

### *Immune-related hub genes in LUAD*

A graphical representation of the study design is shown in *Figure 1*. After differential expression analysis, a total of 8,109 DEGs were obtained. There were 1,864 genes found to be downregulated and 6,245 genes found to be upregulated in the tumor samples (*Figure 2A*). Intersection of the DEGs with the immune genes downloaded from InnateDB and ImmPort (website: <https://cdn.amegroups.com/static/public/jtd-22-494-01.pdf>) yielded 681 immune-related DEGs, with 258 found to be downregulated genes and 423 found to be upregulated genes in tumor samples (*Figure 2B*). Functional enrichment analysis of immune-related DEGs showed that 681 immune-related DEGs were significantly correlated with 1,536 GO items and 56 KEGG pathways (website: <https://cdn.amegroups.com/static/public/jtd-22-494-02.pdf>, *Table S1*). The top 8 GO items and KEGG pathways are displayed in *Figure 2C, 2D*. Immune-related DEGs were enriched in multiple immune responses. Various cell types were found to mediate immunity and complement activation based on GO terms. KEGG pathways analysis showed many were enriched for cytokine signaling, chemokine signaling, and complement pathways. Thus, it was concluded that the screened genes were associated with immunity.

To obtain immune-related hub genes, WGCNA analysis was performed for immune-related DEGs. We first detected outliers in clustering and cut 2 samples by setting the upper limit to 20,000 (*Figure 3A*). The optimal soft-thresholding power was 4, based on the scale-free network (*Figure 3B*). Based on the optimal soft-thresholding and the average linkage hierarchical clustering power, 3 nongray modules containing a total of 588 genes were generated (*Figure 3C, 3D*). Based on the absolute values and P values, the turquoise module, which was most closely related to LUAD, was selected for further analysis. The threshold weight was set to greater than 0.2, and there were 263 genes and 368 edges observable in the turquoise module (*Figure 3E*). Univariate cox regression analysis was performed on 263 genes in the turquoise module and 50 immune-related hub genes were

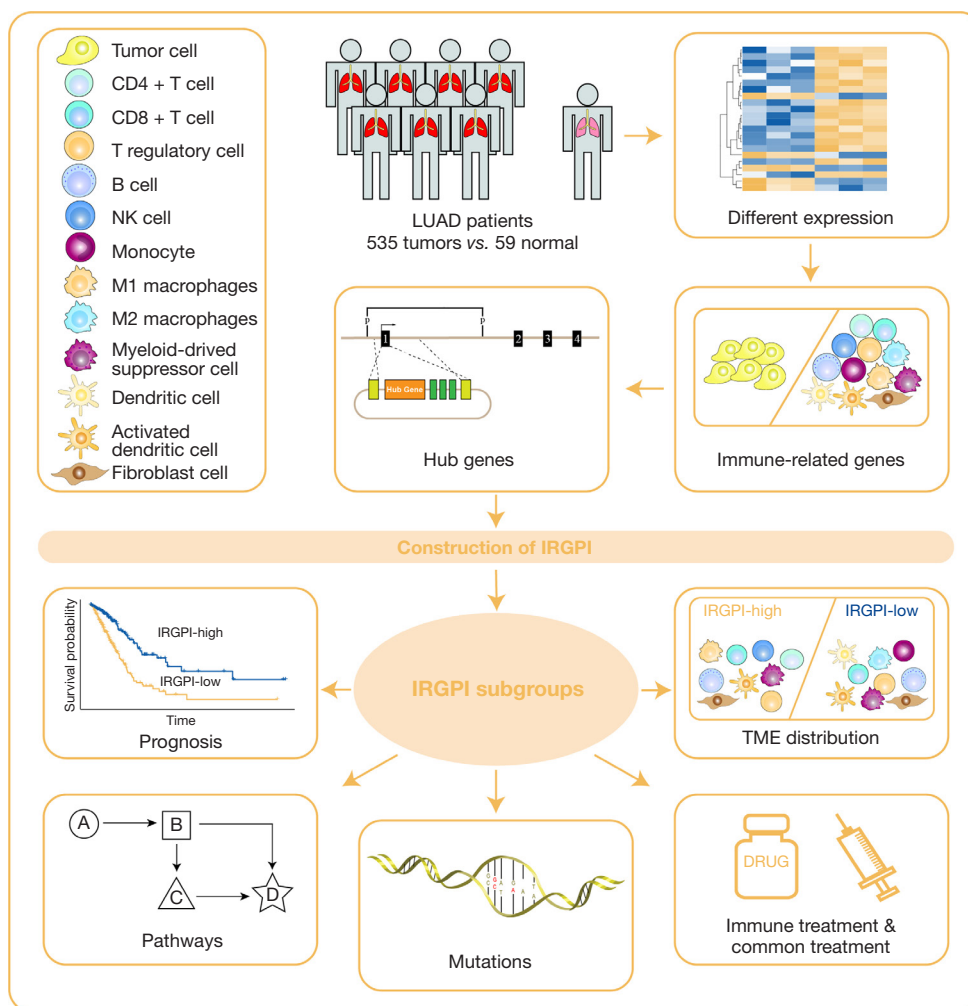


**Figure 1** Graphical representation of the study design. NK, natural killer; LUAD, lung adenocarcinoma; IRGPI, immune-related gene prognostic index; TME, tumor micro environment.

identified that were closely related to the OS of LUAD patients (Figure 4A). Subsequently, to verify the prognostic correlation of hub genes, K-M survival analysis was performed and survival curves for the 16 genes with the highest and lowest prognostic risks are presented in Figure S1.

We then analyzed mutations present in the 50 immune-related hub genes. As shown in Figure S2, most genes contained missense mutations, and some had nonsense mutations, multiple hits, or frameshift deletions. The mutation rates of SEMA4B, C7, and LRRK2 were greater than 4%.

### The IRGPI formula and prognostic value for IRGPI subgroups

We performed multivariate Cox regression analysis on

50 immune-related hub genes to identify independent prognostic genes and obtained 15 genes (*SFTPD*, *S100A16*, *FGF2*, *BIRC5*, *SEMA4B*, *ANGPTL4*, *IL3RA*, *SHC3*, *FCN3*, *TRIM6*, *LRRK2*, *HMGB2*, *RASGEF1B*, *C7*, and *PRKCE*) significantly associated with prognosis (Figure 4B). Next, we used a Cox proportional-hazards model to construct IRGPI based on these genes. The formula of IRGPI was as follows:  $IRGPI = SFTPD \text{ expression} \times (-0.10) + S100A16 \text{ expression} \times 0.24 + FGF2 \text{ expression} \times 0.55 + BIRC5 \text{ expression} \times (-0.22) + SEMA4B \text{ expression} \times 0.27 + ANGPTL4 \text{ expression} \times 0.18 + IL3RA \text{ expression} \times (-0.31) + SHC3 \text{ expression} \times (-0.41) + FCN3 \text{ expression} \times (-0.14) + TRIM6 \text{ expression} \times 0.26 + LRRK2 \text{ expression} \times 0.15 + HMGB2 \text{ expression} \times 0.44 + RASGEF1B \text{ expression} \times (-0.35) + C7 \text{ expression} \times 0.21 + PRKCE \text{ expression} \times 0.38$ .

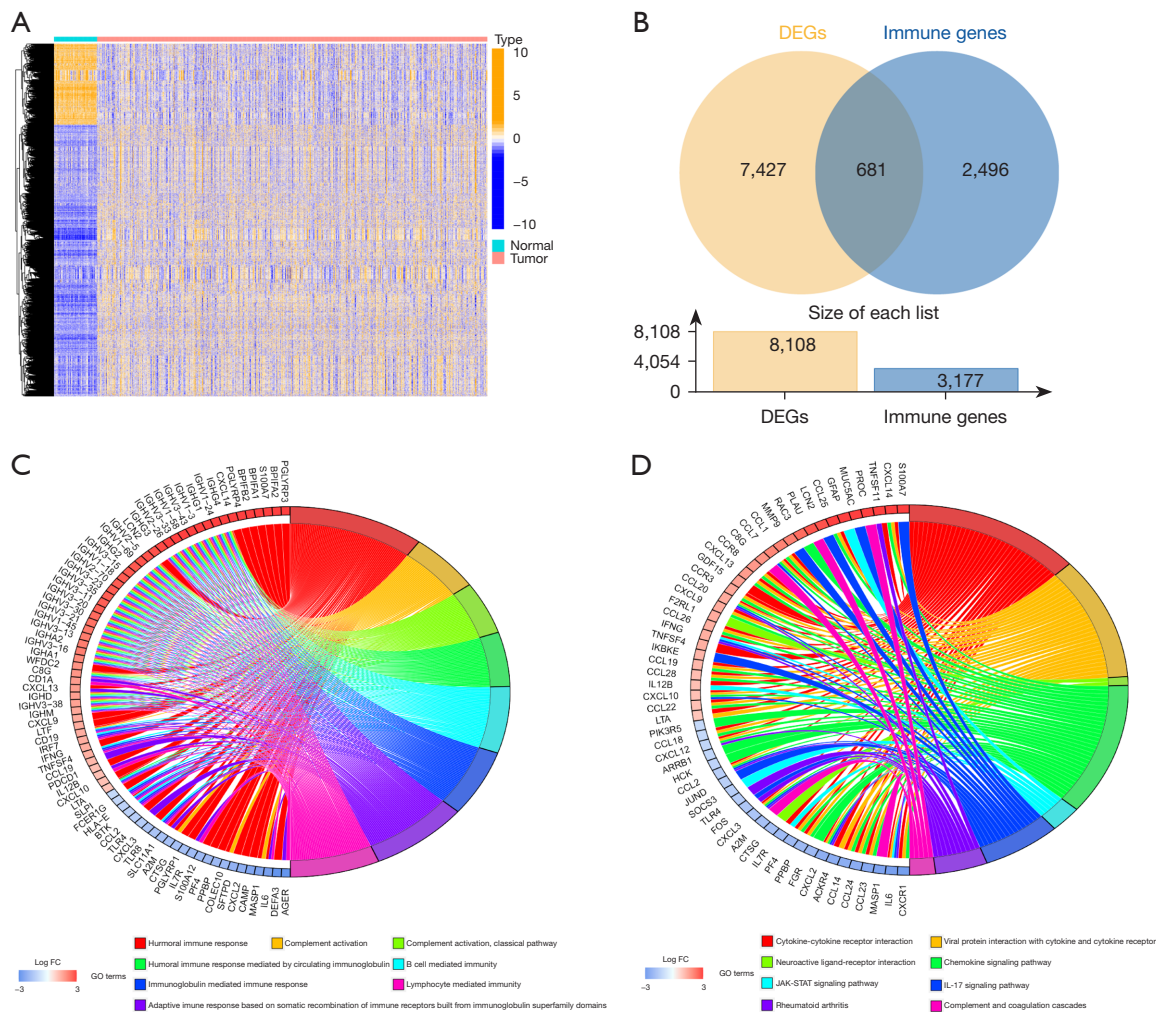


**Figure 2** Differential expression analysis in LUAD patients. (A) Heatmap illustrating all DEGs between 535 tumor samples (red) and 59 normal samples (blue). (B) Venn diagram illustrating 681 immune-related DEGs obtained by the intersection of 8,108 DEGs and 3,177 immune genes. (C) GO enrichment analysis of the immune-related DEGs. (D) KEGG pathway analysis of the immune-related DEGs. DEGs, differentially expressed genes; FC, fold change; GO, Gene Ontology; IL-17, interleukin-17; LUAD, lung adenocarcinoma; KEGG, Kyoto Encyclopedia of Genes and Genomes.

To further confirm that IRGPI could be used as an independent prognostic factor, univariate and multivariate cox regression analyses were performed on IRGPI and other common clinical factors (Table S2). Univariate cox regression analysis showed that IRGPI, tumor (T) stage, metastasis (M) stage, and lymph node (N) stage significantly correlated with the prognosis of LUAD. Multivariate Cox regression analysis confirmed these data. We concluded that IRGPI was an independent prognostic factor after adjusting for other clinicopathological factors.

The median value of IRGPI in the TCGA cohort was

used as the cut-off point to divide patients into high and low IRGPI score subgroups. In the TCGA cohort, the OS of the IRGPI-high subgroup was lower than the IRGPI-low subgroup ( $P < 0.001$ , log-rank test, Figure 4C). The GEO cohort (GSE72094) showed a similar prognosis as the TCGA cohort ( $P = 0.010$ , log-rank test; Figure 4D), confirming the ability of IRGPI to predict OS of LUAD patients.

#### *Molecular characteristics of the IRGPI subgroups*

First, GSEA analysis was performed to identify the enriched

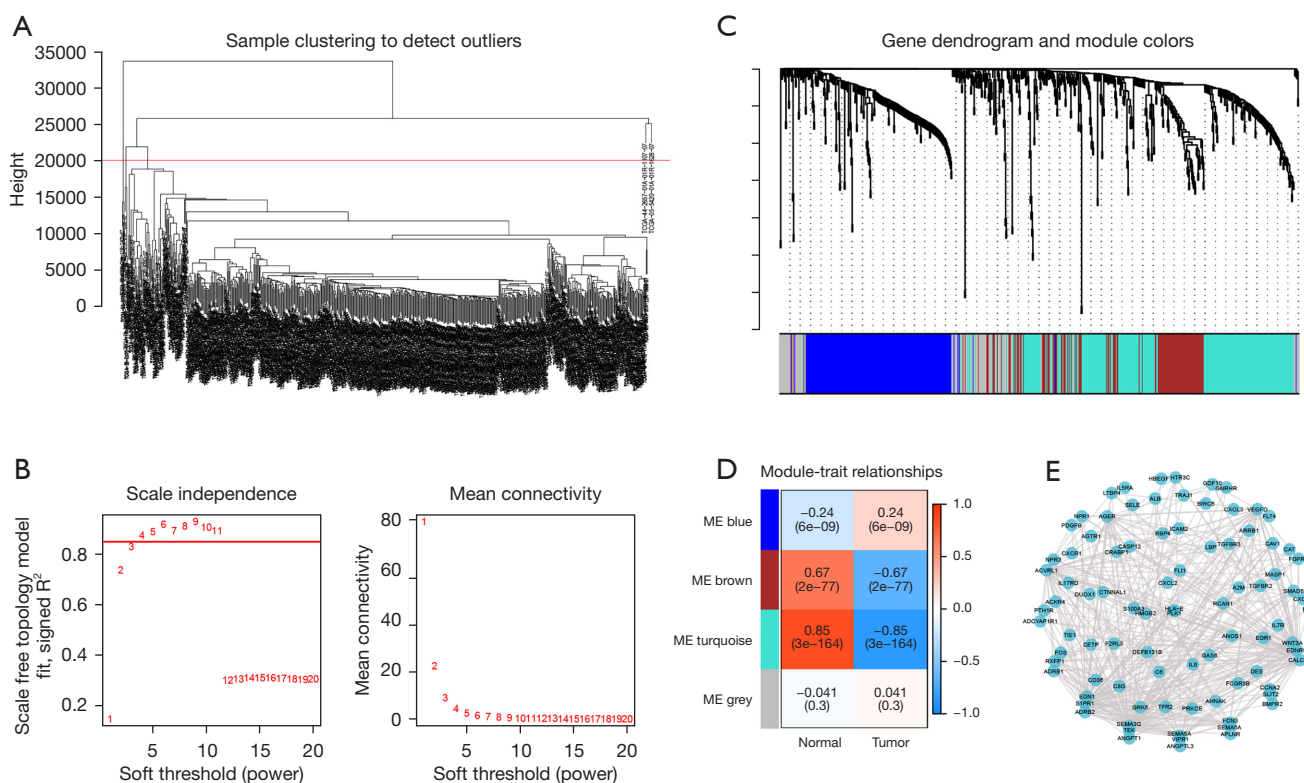


**Figure 3** Identification of hub genes among immune-related DEGs. (A) Two outliers were cut by setting the upper limit at 20,000. (B) The horizontal line in the left graph indicates that the threshold power is 0.85. As shown in the graph, the optimal soft threshold power was 4. (C) The distribution of genes in a dendrogram. (D) Three nongray modules were obtained through WGCNA. (E) The network of the genes in the turquoise module (weight of edge >0.2). ME, module eigengene; DEGs, differentially expressed genes; WGCNA, weighted gene co-expression network analysis.

pathways in the 2 IRGPI subgroups (Table S3). The gene sets of the IRGPI-low subgroup were highly enriched in immune-related pathways (Figure 5A), indicating a better immune environment. However, gene sets of the IRGPI-high subgroup were abundantly enriched in the cell cycle pathway and pathways in cancer (Figure 5B), showing a high correlation with the development of cancer.

We then analyzed mutation data for the 2 subgroups to explore the characteristics from a molecular perspective. We first identified 20 genes with the largest number of mutations, we then analyzed mutation data of the 2 subgroups and displayed the mutation landscapes for the 20 genes (Figure 5C,5D). We found that missense mutations were the most common in both groups, followed by multiple hits and nonsense mutations. The mutation rates of *TP53*, *TTN*, *MUC16*, *RYR2*, *CSMD3*, *LRP1B*, *ZFH4*, *USH2A*, *KRAS*, *XIRP2*, and *FLGA* in the 2 subgroups were

all greater than 20%. The mutations of *TTN* ( $P=0.010$ ) and *PCDH15* ( $P<0.048$ ) genes in the IRGPI-high subgroup were significantly higher than in the IRGPI-low subgroup.

Next, we analyzed the relationship between IRGPI score and PD-L1 expression level and TMB to explore the estimated benefits of ICB therapy. The expression of PD-L1 and TMB in the IRGPI-high subgroup was significantly greater than in the IRGPI-low subgroup ( $P=0.0036$ ,  $P=0.0043$ ; Figure S3A,S3B), suggesting that ICB therapy may result in a better response in IRGPI-high patients.

### Immune characteristics of the 2 IRGPI subgroups

We obtained the TME landscape of LUAD after simulating the infiltration of 22 immune cells and grouped them into 2 IRGPI subgroups (Figure 6A). A comparison of 22 distinct immune cells and common clinical-pathological factors is

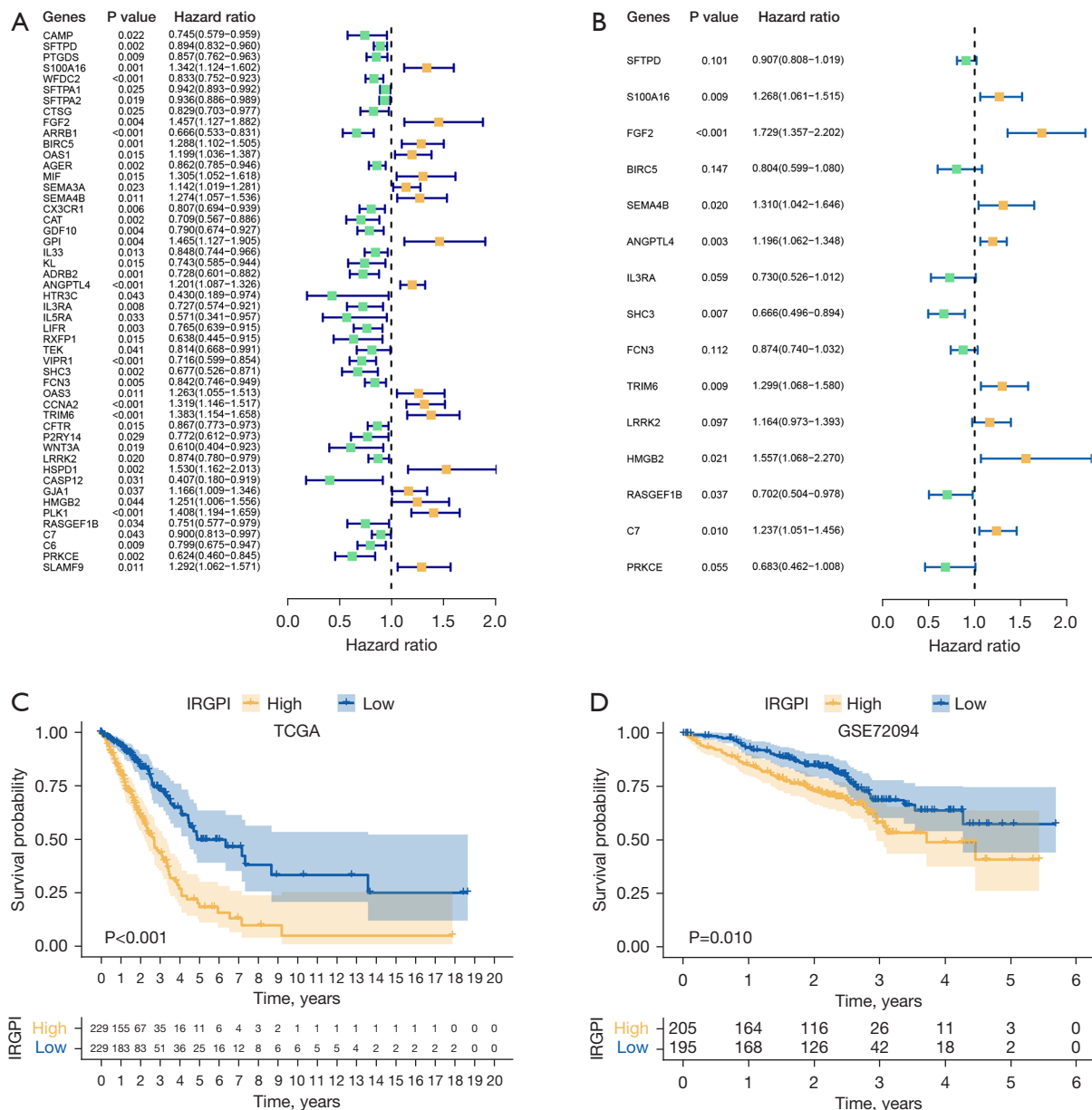


**Figure 4** Prognostic analysis of 2 IRGPI subgroups. (A) Univariate Cox analysis of 50 immune-related hub genes (green dots represent protective factors; yellow dots represent risk factors). (B) Multivariate Cox analysis of 15 constituent genes of IRGPI (green dots represent protective factors; yellow dots represent risk factors). (C) K-M survival curve of different IRGPI subgroups in TCGA cohort. (D) K-M survival curve of different IRGPI subgroups in GEO (GSE72094) cohort. IRGPI immune-related gene prognostic index; TCGA, The Cancer Genome Atlas; K-M, Kaplan-Meier; GEO, Gene Expression Omnibus.

shown in *Figure 6B*. We then used the “limma” package in R to compare the proportion of immune cells in the 2 IRGPI subgroups. The results showed that the abundance of activated memory cluster of differentiation 4 (CD4) T cells, resting natural killer (NK) cells, and macrophages M1

was higher in the IRGPI-high subgroup, while monocytes, macrophages M2, resting dendritic cells, and resting mast cells were widely distributed in the IRGPI-low subgroup (*Figure 6C*). For survival analysis of immune cells with significantly different distributions (*Figure S4*), we observed



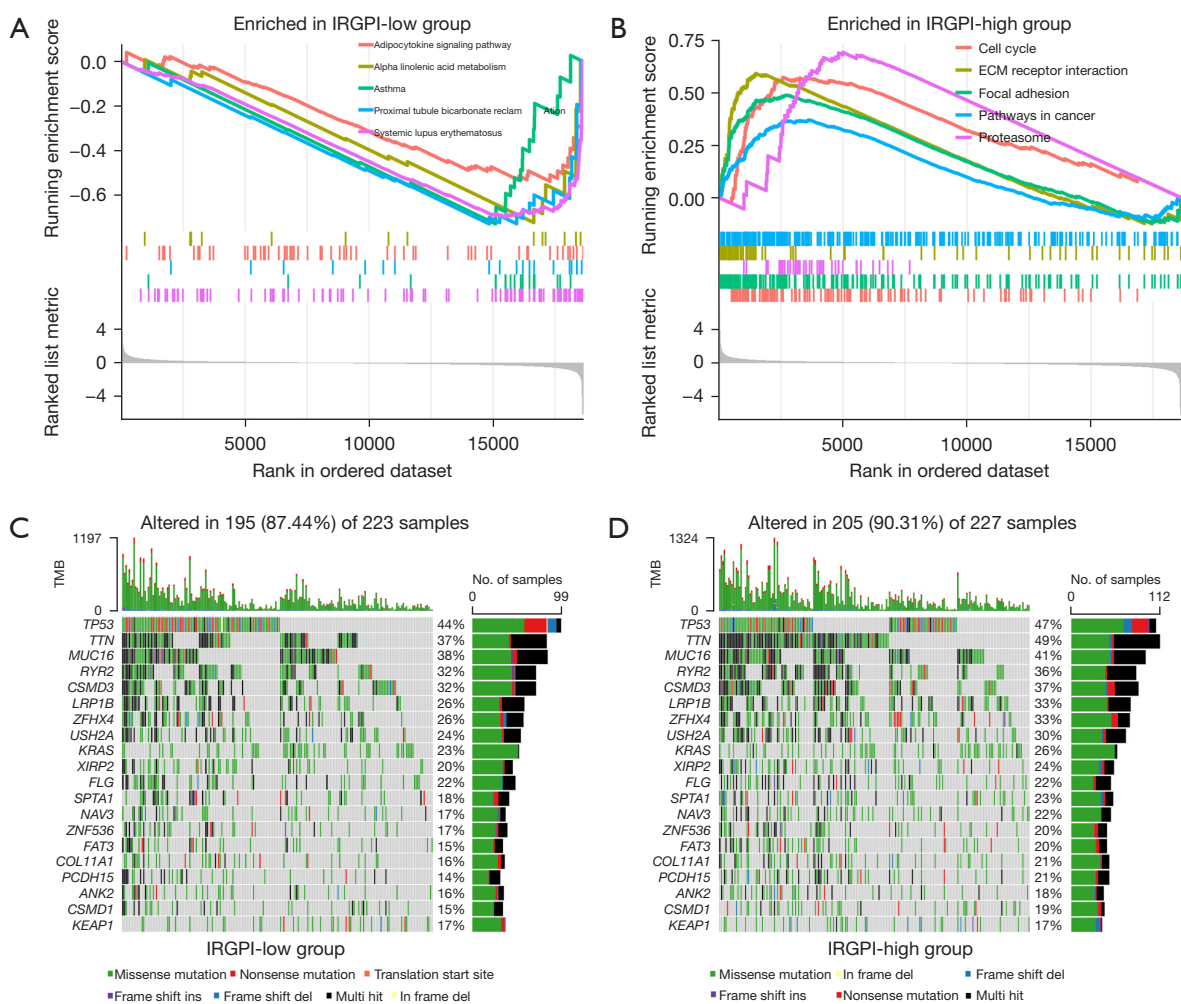


**Figure 5** Molecular characteristics of 2 IRGPI subgroups. (A) Gene sets enriched in IRGPI-low subgroup. (B) Gene sets enriched in IRGPI-high subgroup. (C) Oncoplot displaying the mutation status of IRGPI-low subgroup. Mutated genes are ordered by mutation numbers of the whole sample, with the top 20 genes shown. The colors represent the mutation type. (D) Oncoplot displaying the mutation status of IRGPI-high subgroups. IRGPI, immune-related gene prognostic index; TMB, tumor mutation burden.

that the high expression of activated memory CD4 T cells, resting NK cells, and macrophages M1 resulted in poor prognosis (both  $P < 0.05$ ). In fact, these were all present at a higher abundance in the IRGPI-high subgroup. A higher level of resting dendritic cells predicted a better prognosis ( $P = 0.048$ ), and these were abundant in the IRGPI-low subgroup.

We then defined immune-related function pathway characteristics of the 2 subgroups based on the gene signature. We found that the IRGPI-high subgroup showed greater functions related to antigen presenting cell (APC) co-inhibition, CD8<sup>+</sup> T cells, cytolytic activity, inflammation,

major histocompatibility complex (MHC) class I molecules, para-inflammation, T follicular helper (Tfh) cells, T helper 1 (Th1) cells, and Th2 cells. The IRGPI-high group showed fewer functions related to immature dendritic cells (iDCs), mast cells, and type-II interferon (IFN) response (Figure 6D). In subsequent survival analyses (Figure S5), we found that CD8<sup>+</sup> T cells and Treg enriched in the IRGPI-high subgroup predicted poor prognosis. Higher iDCs, mast cells, and type-II IFN response were associated with better prognosis in the IRGPI-low subgroup. These results also suggested that the prognostic value of IRGPI was related to differential enrichment of immune-related

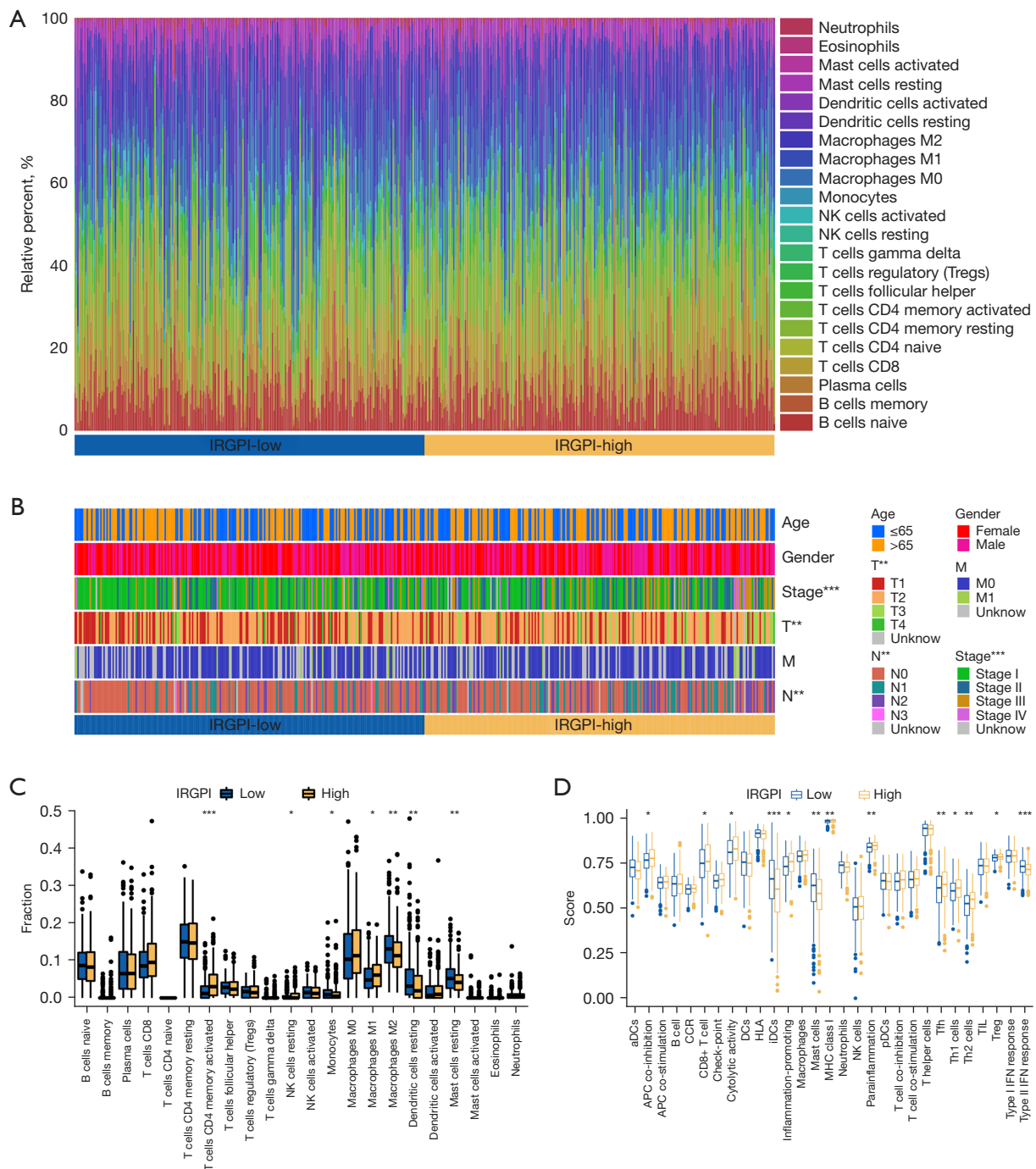


**Figure 6** TME landscape in LUAD patients and the immune characteristics of 2 IRGPI subgroups. (A) The relative percent of 22 immune cells in The Cancer Genome Atlas (TCGA) cohort of 2 IRGPI subgroups. (B) The pathological factors (age, gender, stage, T, M, and N) in the TCGA cohort of 2 IRGPI subgroups (\*\*,  $P < 0.01$ ; \*\*\*,  $P < 0.001$ ). (C) The different fractions of TME cells in 2 IRGPI subgroups. The scattered dots represent the immune fraction of 2 IRGPI subgroups. The thick lines represent the median value. The bottom and top of the boxes are the 25th and 75th percentiles, respectively. “\*\*\*” is used to represent significant statistical differences between the 2 subgroups (\*,  $P < 0.05$ ; \*\*,  $P < 0.01$ ; \*\*\*,  $P < 0.001$ ). (D) The different enrichment scores of immune-related functions in 2 IRGPI subgroups (\*,  $P < 0.05$ ; \*\*,  $P < 0.01$ ; \*\*\*,  $P < 0.001$ ). NK, natural killer; IRGPI, immune-related gene prognostic index; T, tumor; M, metastasis; N, lymph node; TME, tumor micro environment; LUAD, lung adenocarcinoma; TCGA, The Cancer Genome Atlas.

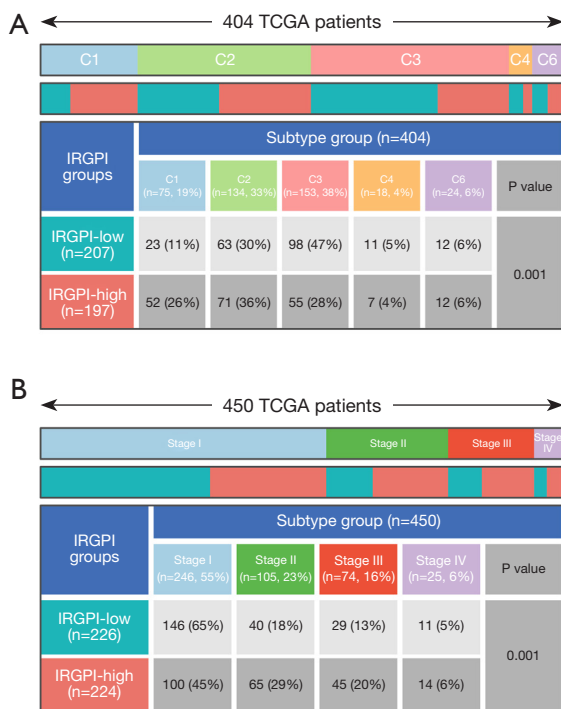


**Figure 7** Distribution of immune and clinical subtypes in 2 IRGPI subgroups. (A) Heatmap and table showing the distribution of LUAD patients by immune subtype (C1, C2, C3, C4, and C6) between 2 IRGPI subgroups. (B) Heatmap and table showing the distribution of LUAD patients by clinical stage (stage I, stage II, stage III, and stage IV) between 2 IRGPI subgroups. TCGA, The Cancer Genome Atlas; IRGPI, immune-related gene prognostic index; LUAD, lung adenocarcinoma.

function pathways.

### Relationship between IRGPI, immune subtypes, and clinical stage

Tumor samples from the TCGA were divided into 6 immune subtypes according to immune characteristics: C1 (wound healing), C2 (IFN- $\gamma$  dominant), C3 (inflammatory), C4 (lymphocyte depleted), C5 (immunologically quiet), and C6 [transforming growth factor (TGF)- $\beta$  dominant] (16). As shown in *Figure 7A*, there was a significant difference in the distribution of immune subtypes between the 2 subgroups ( $P=0.001$ ). The proportion of the C1 subtype was greater in the IRGPI-high subgroup, and the proportion of the C3 subtype was greater in the IRGPI-low subgroup.

As for clinical stages, there was a significant difference in the distribution between the 2 subgroups ( $P=0.001$ ;

*Figure 7B*). The proportions of stage II and stage III in the IRGPI-high subgroup were high. In contrast, the proportion of stage I was high in the IRGPI-low subgroup. As a result, the IRGPI-high subgroup showed higher clinical stage, representing severe disease state and poor prognosis.

### The relationship between IRGPI and ICB therapy or common treatments

TIDE was based on comprehensive analysis of the tumor expression spectrum to predict the efficacy of ICB therapy and was more accurate than PD-L1 expression and TMB (22). As shown in *Figure 8A*, we found that the T-cell dysfunction score of the IRGPI-high subgroup was higher than the IRGPI-low subgroup ( $P<0.001$ ), suggesting that T cell-mediated immune processes may have been impaired in IRGPI-high patients (23,24). Benefits of ICB therapy showed no difference in the 2 subgroups since they had similar TIDE scores.

As shown in *Figure 8B*, we found that the AUCs of 1-, 2- and 3-year follow-up were all higher than 0.70 in the time-dependent ROC curve of IRGPI. This suggested that IRGPI was an important prognostic indicator. When comparing TIDE and TIS, the AUC of IRGPI was higher than TIDE and TIS at all follow-up times, showing that IRGPI had a better prognostic value than traditional biomarkers.

IRGPI had the ability to guide personalized treatment of LUAD based on drug susceptibility data for multiple treatments in the 2 subgroups through GDSC (*Figure 8C*). We found that the IC<sub>50</sub> of 8 chemotherapeutic agents (paclitaxel, gemcitabine, epothilone B, cytarabine, docetaxel, vinblastine, cisplatin, and etoposide) in the IRGPI-high subgroup were significantly lower than in the IRGPI-low subgroup (both  $P<0.05$ ), indicating that the response and efficacy of IRGPI-high patients to chemotherapy may be better. The IC<sub>50</sub> values of the chemotherapy drug Vinorelbine and 3 molecular-targeted therapy drugs (erlotinib, gefitinib, and BIBW2992) showed no significant differences between the 2 subgroups ( $P>0.05$ ).

### Discussion

ICB therapy is very effective in the treatment of LUAD and various other cancers (11,25,26). However, the efficacy of ICB therapy is variable in different tumors and patients (11-15). Determining which patients will respond well to

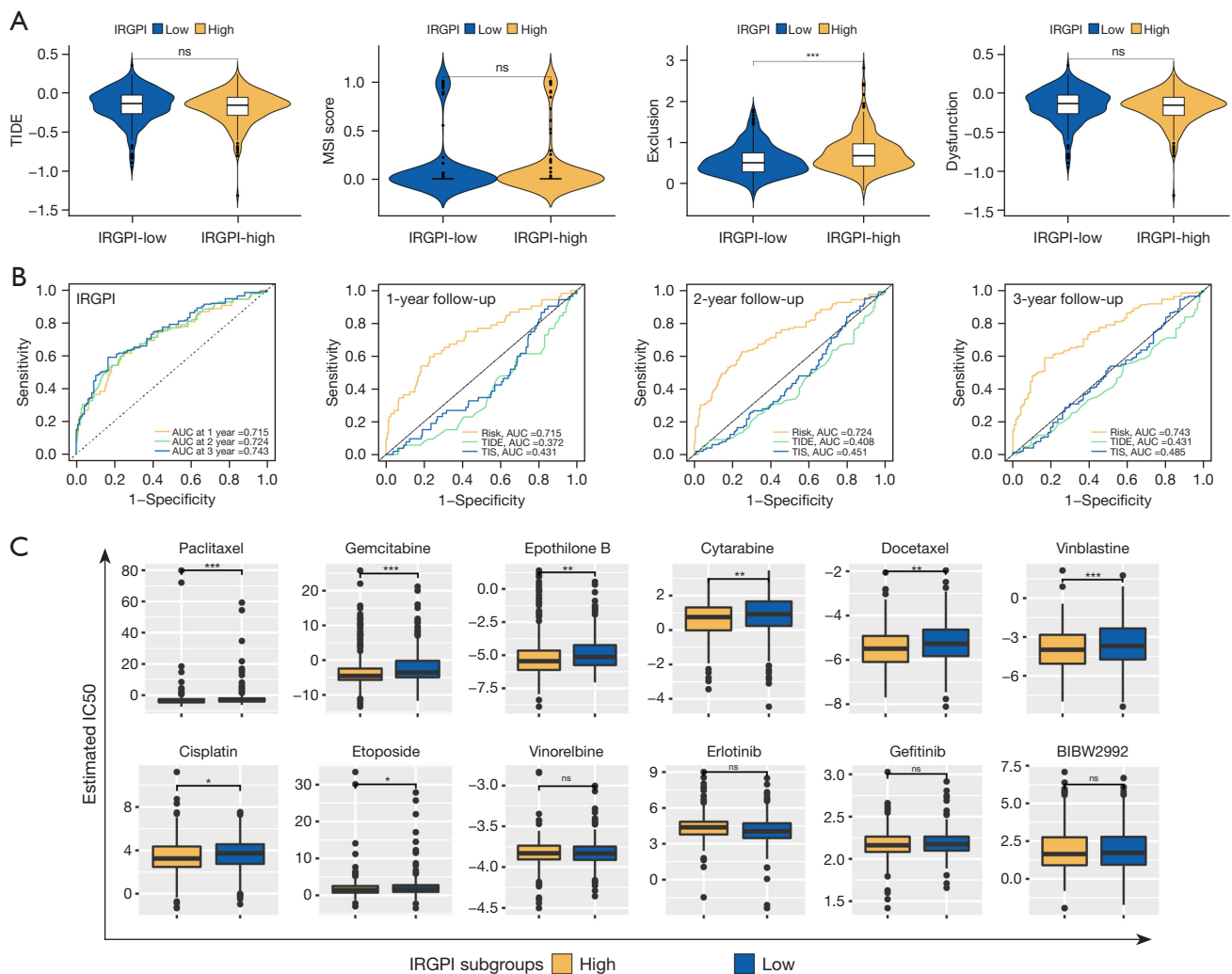


**Figure 8** The prognostic value and response to therapies of the IRGPI. (A) TIDE, MSI, T-cell exclusion, and T-cell dysfunction score in 2 IRGPI subgroups (ns, no significance; \*\*\*,  $P < 0.001$ ). (B) Time-dependent ROC analysis of IRGPI, TIS, and TIDE on OS at 1-, 2-, 3-year follow-up in TCGA cohort. (C) Drug sensitivity of 12 drugs between 2 IRGPI subgroups (ns, no significance; \*,  $P < 0.05$ ; \*\*,  $P < 0.01$ ; \*\*\*,  $P < 0.001$ ). IRGPI, immune-related gene prognostic index; TIDE, Tumor Immune Dysfunction and Exclusion; AUC, areas under the curve; IC50, half-maximal inhibitory concentration; TIS, tumor inflammation signature; MSI, microsatellite instability; ROC, receiver operating characteristic; OS, overall survival; TCGA, The Cancer Genome Atlas.

ICB therapy is necessary. Due to complex variations in the TME, it is difficult to identify a single factor biomarker that can predict response to multiple treatments. Yin *et al.*, Shen *et al.*, and Chen *et al.* developed prognostic biomarkers for head and neck squamous cell carcinoma, ovarian cancer, and clear cell renal cell carcinoma based on immune-related genes (27-29). However, there are no relevant studies looking into biomarkers for LUAD. Therefore, it is necessary to develop a biomarker based on the expression of multiple immune-related genes to guide LUAD treatment

strategies (30).

WGCNA is an analysis method that can find co-expressed immune-related genes, allowing us to explore potential biomarkers and focus on hub genes. We obtained 50 immune-related hub genes significantly associated with OS through WGCNA and survival analysis and constructed IRGPI based on 15 independent prognostic genes. In LUAD patients, IRGPI demonstrated a good association with prognosis. For example, IRGPI-high patients had poor prognosis, while IRGPI-low patients showed better

prognosis. The results were confirmed using TCGA and GEO cohorts, concluding that IRGPI is a valuable immune-related biomarker for LUAD that can be used to predict prognosis and guide treatment decisions.

IRGPI is based on 15 genes (*SFTPD*, *S100A16*, *FGF2*, *BIRC5*, *SEMA4B*, *ANGPTL4*, *IL3RA*, *SHC3*, *FCN3*, *TRIM6*, *LRRK2*, *HMGB2*, *RASGEF1B*, *C7*, and *PRKCE*). Pulmonary surfactant-associated protein (SP-D) encoded by surfactant protein D (SFTPD) shows dual effects of suppressing or enhancing inflammation through binding different receptors (31). SP-D can inhibit the proliferation, invasion, and migration of LUAD cells by interacting with epidermal growth factor receptor (EGFR) (32). Fibroblast growth factor-2 (FGF-2), a member of the FGF family, promotes proliferation, repair, and migration in a variety of cells (33). The S100 protein family has shown a correlation with various signaling pathways in cancer cells, and proteomics have reported that S100A16 significantly correlated with poor prognosis of LUAD patients (34). Semaphoring 4B (SEMA4B) belongs to the semaphorin protein family, which regulates cell migration, angiogenesis, and immune response. According to the report, SEMA4B may have promoted the expression of matrix metalloproteinase-9 (MMP9) by activating the phosphatidylinositol 3-kinase (PI3K) signaling pathway. An increase in metastasis promotes NSCLC (35). Baculoviral inhibitor of apoptosis repeat-containing 5 (BIRC5, also as known as survivin), an inhibitor of apoptosis-related proteins, is expressed in the growth 2 (G2)/mitosis (M) checkpoint phase. Overexpression of BIRC5 in cancer is conducive to its aberrant progression (36). Alpha subunit of interleukin 3 receptor (IL3RA) is a cell membrane protein produced by activated T lymphocytes and plays a role in immunity and hematopoiesis. RasGEF1, a member of the guanine-nucleotide exchange factor (GEF) family, is induced in macrophages by stimulation of Toll-like receptor (TLR). Repression of RasGEF1B reduces intercellular adhesion molecule 1 (ICAM-1) expression. This plays a role in the immune response by promoting the binding of leukocytes to endotheliocytes and their subsequent migration into tissues (37). Both ficolin-3 (encoded by FCN) and complement component 7 (C7) are involved in the complement system and play key roles in immune-inflammatory responses. In summary, IRGPI fully reflects the progression of LUAD proliferation, invasion, metastasis, angiogenesis, and multiple other tumor development processes. It is widely associated with various aspects of the immune response. As a multifactor and multiperspective

biomarker, IRGPI is a better prognostic indicator than traditional biomarkers that can only narrowly reflect a single perspective of the tumor.

Somatic mutations are related to tumor cell sensitivity and anti-chemotherapy mechanisms. These mutations play a major role in predicting an antitumor drug response (38). The mutant gene showing the greatest difference in the 2 groups was TTN. More specifically, the IRGPI-high subgroup showed a greater TTN mutation rate than the IRGPI-low subgroup. One study (39) found that long noncoding RNA (lncRNA) titan-antisense RNA1 (TTN-AS1) transcribed in TTN antisense chain is upregulated in LUAD, and TTN-AS1 binds to microRNA (miR)-142-5p as a competing endogenous RNA (ceRNA) to indirectly upregulate cyclin-dependent kinase 5 (CDK5) expression. Knockdown of TTN-AS1 significantly reduced the proliferation, invasion, and migration of LUAD cells. This research suggested that TTN mutations may have been associated with the relatively poor prognosis of the IRGPI-high subgroup and could be a potential target for the treatment of IRGPI-high patients.

TME plays an important role in the ICB therapy response as well as LUAD patient prognosis. Our study revealed that there were significant differences in the infiltration of some immune cells between the 2 subgroups. These differences determined the heterogeneity of the TME and affected patient outcomes. Previous studies have found that both T-cells and NK cells have antitumor effects and are positively correlated with prognosis in cases of high-level infiltration (40,41). The main subtype of macrophages in most tumors is M2, which usually promotes proliferation and invasion that leads to poor prognosis. In contrast, the degree of infiltration of M1 macrophages positively correlates with prognosis (42). Results from our study supported these conclusions, including the proportion of various immune cells and also the location and activity of immune cells affecting immune response and ultimately prognosis. The exploration of deep TME characteristics of the 2 IRGPI subgroups is needed in future studies.

There were significant differences in the C1 and C3 immune subtypes between the 2 groups. The C1 subtype highly expresses angiogenic genes and contains a high tumor proliferation rate. The C3 subtype is characterized by abundant Th17 cells and Th1 cell infiltration, shows mild to moderate tumor proliferation rates, and contains low levels of somatic copy number variation and aneuploidy. In a previous study (16), the C3 subtype was linked to a better prognosis compared to the C1 subtype. This led to the conclusion that prognosis may be better in the IRGPI-

low compared to the IRGPI-high subgroup. There were also significant differences observed in the distribution of clinical stages for the 2 subgroups. A higher clinical stage suggested that patients in the IRGPI-high subgroup were more likely to have poor prognosis. The results of these analyses are consistent with the prognostic results of IRGPI and are helpful for physicians to predict the immune type characteristics and disease progression of LUAD patients.

PD-L1 and TMB are 2 classic biomarkers commonly used in clinical practice, with both having a positive correlation with the response of ICB-treated patients (43). In our study, the expression levels of PD-L1 and TMB were significantly higher in the IRGPI-high subgroup, suggesting that patients in the IRGPI-high subgroup would better benefit from ICB therapy. In comparing IRGPI with TIDE and TIS, IRGPI was shown to be an excellent prognostic indicator with better predictability. IRGPI overcame the one-sided reflection of traditional biomarkers for prognosis, making it a promising biomarker for clinical application.

GDSC links complex genomes with drug sensitivity and facilitates the discovery of new biomarkers related to drug response (44). GDSC analysis showed that the IRGPI-high group would have a better response to chemotherapy and higher benefits in response to ICB therapy. The application of ICB therapy in combination with chemotherapy should be considered to improve the poor prognosis of IRGPI-high patients. The combined use of multiple therapies showed better effects in enhancing drug response and delaying drug resistance.

In future clinical application of IRGPI, a large amount of information for LUAD patients, such as reliable prediction of prognosis, TME landscape, estimation of clinical stage before cancer-related checkup, and benefits of multiple therapies can be predicted. This will help to determine the optimal treatment strategy. We are more inclined to recommend a combinational strategy including ICB therapy and chemotherapy for patients with high IRGPI scores. Meanwhile, our study needs further real-world research validation, which is the direction of our follow-up research.

## Conclusions

In conclusion, we developed a biomarker with excellent prospects for clinical practice to help guide immunotherapy. IRGPI surpassed the limitations of traditional biomarkers and reduced bias of prognostic models through the use of immune-related hub DEGs, demonstrating powerful prognosis predictability. IRGPI can predict LUAD patient

response to ICB therapy and traditional treatments, increasing the value of this biomarker in allowing for individualized treatment regimens.

## Acknowledgments

We thank the CIBERSORT and TIDE websites for providing online tools for immune infiltration analysis and immunotherapy predictive efficacy analysis.

*Funding:* None.

## Footnote

*Reporting Checklist:* The authors have completed the TRIPOD reporting checklist. Available at <https://jtd.amegroups.com/article/view/10.21037/jtd-22-494/rc>

*Conflicts of Interest:* All authors have completed the ICMJE uniform disclosure form (available at <https://jtd.amegroups.com/article/view/10.21037/jtd-22-494/coif>). The authors have no conflicts of interest to declare.

*Ethical Statement:* The authors are accountable for all aspects of the work in ensuring that questions related to the accuracy or integrity of any part of the work are appropriately investigated and resolved. The study was conducted in accordance with the Declaration of Helsinki (as revised in 2013).

*Open Access Statement:* This is an Open Access article distributed in accordance with the Creative Commons Attribution-NonCommercial-NoDerivs 4.0 International License (CC BY-NC-ND 4.0), which permits the non-commercial replication and distribution of the article with the strict proviso that no changes or edits are made and the original work is properly cited (including links to both the formal publication through the relevant DOI and the license). See: <https://creativecommons.org/licenses/by-nc-nd/4.0/>.

## References

1. Siegel RL, Miller KD, Fuchs HE, et al. Cancer Statistics, 2021. *CA Cancer J Clin* 2021;71:7-33.
2. Hua X, Zhao W, Pesatori AC, et al. Genetic and epigenetic intratumor heterogeneity impacts prognosis of lung adenocarcinoma. *Nat Commun* 2020;11:2459.
3. Miller M, Hanna N. Advances in systemic therapy for non-small cell lung cancer. *BMJ* 2021;375:n2363.

4. Girard N, Perol M, Simon G, et al. Treatment strategies for unresectable locally advanced non-small cell lung cancer in the real-life ESME cohort. *Lung Cancer* 2021;162:119-27.
5. Yu HA, Suzawa K, Jordan E, et al. Concurrent Alterations in EGFR-Mutant Lung Cancers Associated with Resistance to EGFR Kinase Inhibitors and Characterization of MTOR as a Mediator of Resistance. *Clin Cancer Res* 2018;24:3108-18.
6. Marusyk A, Janiszewska M, Polyak K. Intratumor Heterogeneity: The Rosetta Stone of Therapy Resistance. *Cancer Cell* 2020;37:471-84.
7. Pardoll DM. The blockade of immune checkpoints in cancer immunotherapy. *Nat Rev Cancer* 2012;12:252-64.
8. Mellman I, Coukos G, Dranoff G. Cancer immunotherapy comes of age. *Nature* 2011;480:480-9.
9. Sharma P, Allison JP. The future of immune checkpoint therapy. *Science* 2015;348:56-61.
10. Morad G, Helmink BA, Sharma P, et al. Hallmarks of response, resistance, and toxicity to immune checkpoint blockade. *Cell* 2021;184:5309-37.
11. Gettinger SN, Horn L, Gandhi L, et al. Overall Survival and Long-Term Safety of Nivolumab (Anti-Programmed Death 1 Antibody, BMS-936558, ONO-4538) in Patients With Previously Treated Advanced Non-Small-Cell Lung Cancer. *J Clin Oncol* 2015;33:2004-12.
12. Herbst RS, Baas P, Kim DW, et al. Pembrolizumab versus docetaxel for previously treated, PD-L1-positive, advanced non-small-cell lung cancer (KEYNOTE-010): a randomised controlled trial. *Lancet* 2016;387:1540-50.
13. Rizvi NA, Mazières J, Planchard D, et al. Activity and safety of nivolumab, an anti-PD-1 immune checkpoint inhibitor, for patients with advanced, refractory squamous non-small-cell lung cancer (CheckMate 063): a phase 2, single-arm trial. *Lancet Oncol* 2015;16:257-65.
14. Garon EB, Rizvi NA, Hui R, et al. Pembrolizumab for the treatment of non-small-cell lung cancer. *N Engl J Med* 2015;372:2018-28.
15. Borghaei H, Paz-Ares L, Horn L, et al. Nivolumab versus Docetaxel in Advanced Nonsquamous Non-Small-Cell Lung Cancer. *N Engl J Med* 2015;373:1627-39.
16. Thorsson V, Gibbs DL, Brown SD, et al. The Immune Landscape of Cancer. *Immunity* 2018;48:812-830.e14.
17. Smyth GK, Ritchie M, Thorne N, et al. limma: Linear Models for Microarray Data. 2010. Available online: [http://doi.org/10.1007/0-387-29362-0\\_23](http://doi.org/10.1007/0-387-29362-0_23)
18. Yu G, Wang LG, Han Y, et al. clusterProfiler: an R package for comparing biological themes among gene clusters. *OMICS* 2012;16:284-7.
19. Langfelder P, Horvath S. WGCNA: an R package for weighted correlation network analysis. *BMC Bioinformatics* 2008;9:559.
20. Mayakonda A, Lin DC, Assenov Y, et al. Maftools: efficient and comprehensive analysis of somatic variants in cancer. *Genome Res* 2018;28:1747-56.
21. Hänzelmann S, Castelo R, Guinney J. GSEA: gene set variation analysis for microarray and RNA-seq data. *BMC Bioinformatics* 2013;14:7.
22. Jiang P, Gu S, Pan D, et al. Signatures of T cell dysfunction and exclusion predict cancer immunotherapy response. *Nat Med* 2018;24:1550-8.
23. Sharma P, Wagner K, Wolchok JD, et al. Novel cancer immunotherapy agents with survival benefit: recent successes and next steps. *Nat Rev Cancer* 2011;11:805-12.
24. Schreiber RD, Old LJ, Smyth MJ. Cancer immunoediting: integrating immunity's roles in cancer suppression and promotion. *Science* 2011;331:1565-70.
25. Brahmer JR, Tykodi SS, Chow LQ, et al. Safety and activity of anti-PD-L1 antibody in patients with advanced cancer. *N Engl J Med* 2012;366:2455-65.
26. Robert C, Thomas L, Bondarenko I, et al. Ipilimumab plus dacarbazine for previously untreated metastatic melanoma. *N Engl J Med* 2011;364:2517-26.
27. Yin X, Wang Z, Wang J, et al. Development of a novel gene signature to predict prognosis and response to PD-1 blockade in clear cell renal cell carcinoma. *Oncoimmunology* 2021;10:1933332.
28. Shen S, Wang G, Zhang R, et al. Development and validation of an immune gene-set based Prognostic signature in ovarian cancer. *EBioMedicine* 2019;40:318-26.
29. Chen Y, Li ZY, Zhou GQ, et al. An Immune-Related Gene Prognostic Index for Head and Neck Squamous Cell Carcinoma. *Clin Cancer Res* 2021;27:330-41.
30. Frederick DT, Piris A, Cogdill AP, et al. BRAF inhibition is associated with enhanced melanoma antigen expression and a more favorable tumor microenvironment in patients with metastatic melanoma. *Clin Cancer Res* 2013;19:1225-31.
31. Gardai SJ, Xiao YQ, Dickinson M, et al. By binding SIRPalpha or calreticulin/CD91, lung collectins act as dual function surveillance molecules to suppress or enhance inflammation. *Cell* 2003;115:13-23.
32. Hasegawa Y, Takahashi M, Ariki S, et al. Surfactant protein D suppresses lung cancer progression by downregulation of epidermal growth factor signaling. *Oncogene* 2015;34:838-45.

33. Bikfalvi A, Klein S, Pintucci G, et al. Biological roles of fibroblast growth factor-2. *Endocr Rev* 1997;18:26-45.
34. Kobayashi M, Nagashio R, Saito K, et al. Prognostic significance of S100A16 subcellular localization in lung adenocarcinoma. *Hum Pathol* 2018;74:148-55.
35. Jian H, Zhao Y, Liu B, et al. SEMA4b inhibits MMP9 to prevent metastasis of non-small cell lung cancer. *Tumour Biol* 2014;35:11051-6.
36. Ambrosini G, Adida C, Altieri DC. A novel anti-apoptosis gene, survivin, expressed in cancer and lymphoma. *Nat Med* 1997;3:917-21.
37. Ng WL, Marinov GK, Liau ES, et al. Inducible RasGEF1B circular RNA is a positive regulator of ICAM-1 in the TLR4/LPS pathway. *RNA Biol* 2016;13:861-71.
38. Kim N, He N, Kim C, et al. Systematic analysis of genotype-specific drug responses in cancer. *Int J Cancer* 2012;131:2456-64.
39. Jia Y, Duan Y, Liu T, et al. LncRNA TTN-AS1 promotes migration, invasion, and epithelial mesenchymal transition of lung adenocarcinoma via sponging miR-142-5p to regulate CDK5. *Cell Death Dis* 2019;10:573.
40. Zhao S, Li C, Ye Y, et al. Expression of Chemerin Correlates With a Favorable Prognosis in Patients With Non-Small Cell Lung Cancer. *Laboratory Medicine* 2011;42:553-7.
41. Huang SM, Wu SP, Liao RQ, et al. P2.03b-043 Peripheral Blood CD45RA+ CCR7+ Naive T Cells Were Correlated with Prognosis in Non-Small Cell Lung Cancer Patients. *J Thorac Oncol* 2017;12:S961-2.
42. Josephs DH, Bax HJ, Karagiannis SN. Tumour-associated macrophage polarisation and re-education with immunotherapy. *Front Biosci (Elite Ed)* 2015;7:293-308.
43. Topalian SL, Hodi FS, Brahmer JR, et al. Safety, activity, and immune correlates of anti-PD-1 antibody in cancer. *N Engl J Med* 2012;366:2443-54.
44. Yang W, Soares J, Greninger P, et al. Genomics of Drug Sensitivity in Cancer (GDSC): a resource for therapeutic biomarker discovery in cancer cells. *Nucleic Acids Res* 2013;41:D955-61.

(English Language Editor: A. Muylwyk)

**Cite this article as:** Wang C, Lu T, Xu R, Chang X, Luo S, Peng B, Wang J, Yao L, Wang K, Shen Z, Zhao J, Zhang L. A bioinformatics-based immune-related prognostic index for lung adenocarcinoma that predicts patient response to immunotherapy and common treatments. *J Thorac Dis* 2022;14(6):2131-2146. doi: 10.21037/jtd-22-494



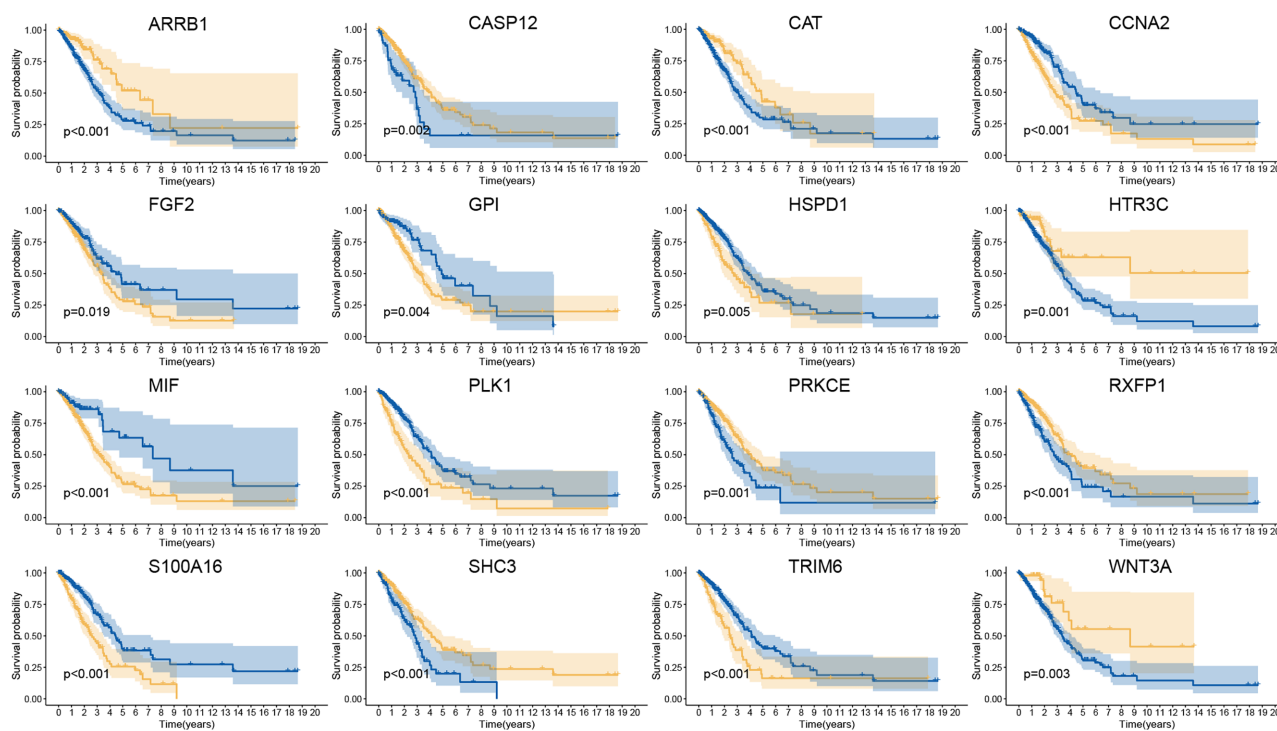
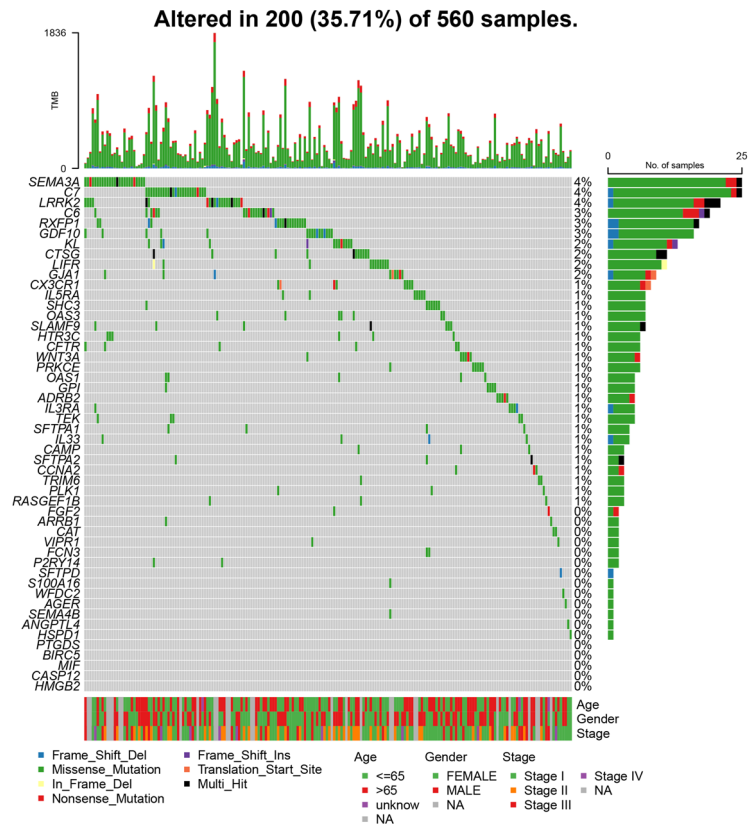
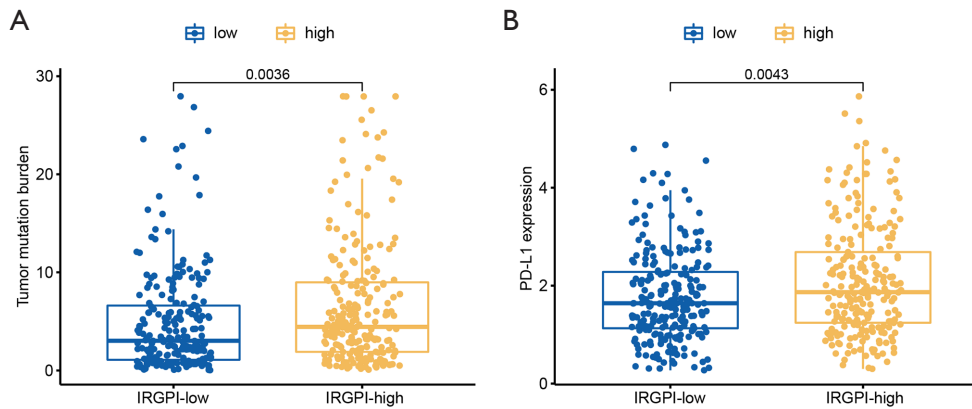


Figure S1 Kaplan-Meier (K-M) survival curve of differential expression groups in 16 genes out of 50 immune-related hub genes.



**Figure S2** Oncoplot displaying the mutation status of 50 immune-related hub genes in The Cancer Genome Atlas (TCGA) cohort. Mutated genes are ordered by mutation numbers of the whole sample, the colors represent the mutation type. TMB, tumor mutation burden.



**Figure S3** The relationship between immune-related gene prognostic index (IRGPI) and tumor mutation burden and programmed death-ligand 1 (PD-L1) expression. (A) Differential analysis of tumor mutation burden in 2 IRGPI subgroups. (B) Differential analysis of PD-L1 expression in 2 IRGPI subgroups.

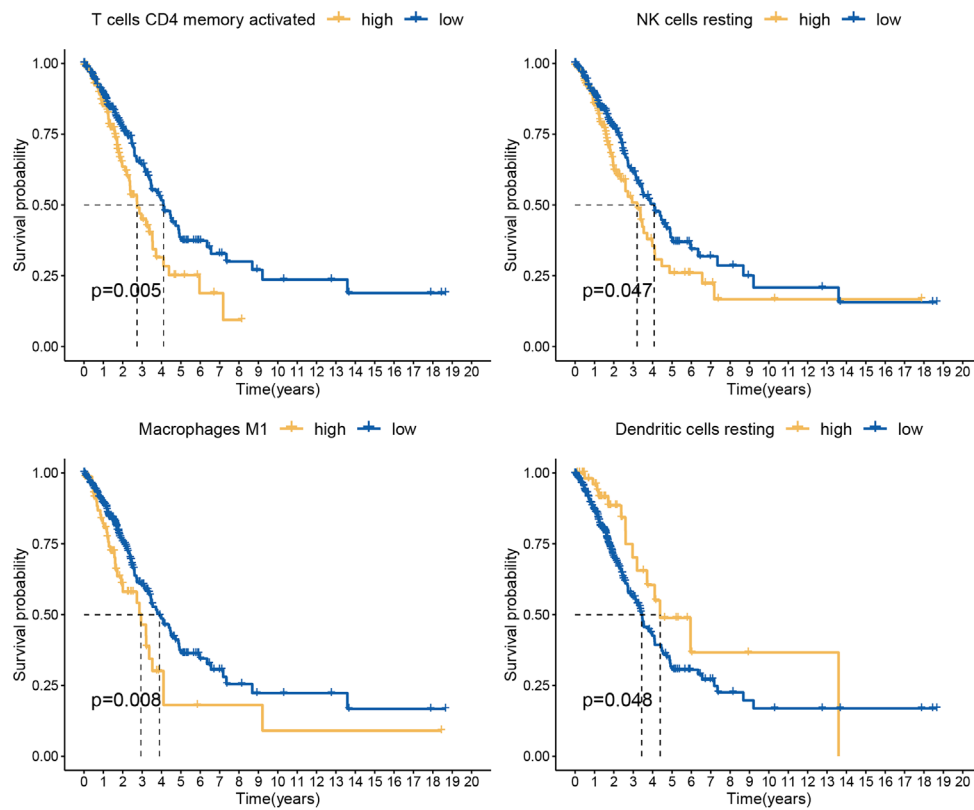


**Figure S4** Kaplan-Meier (K-M) survival analysis of immune cells with different distributions in 2 immune-related gene prognostic index (IRGPI) subgroups.

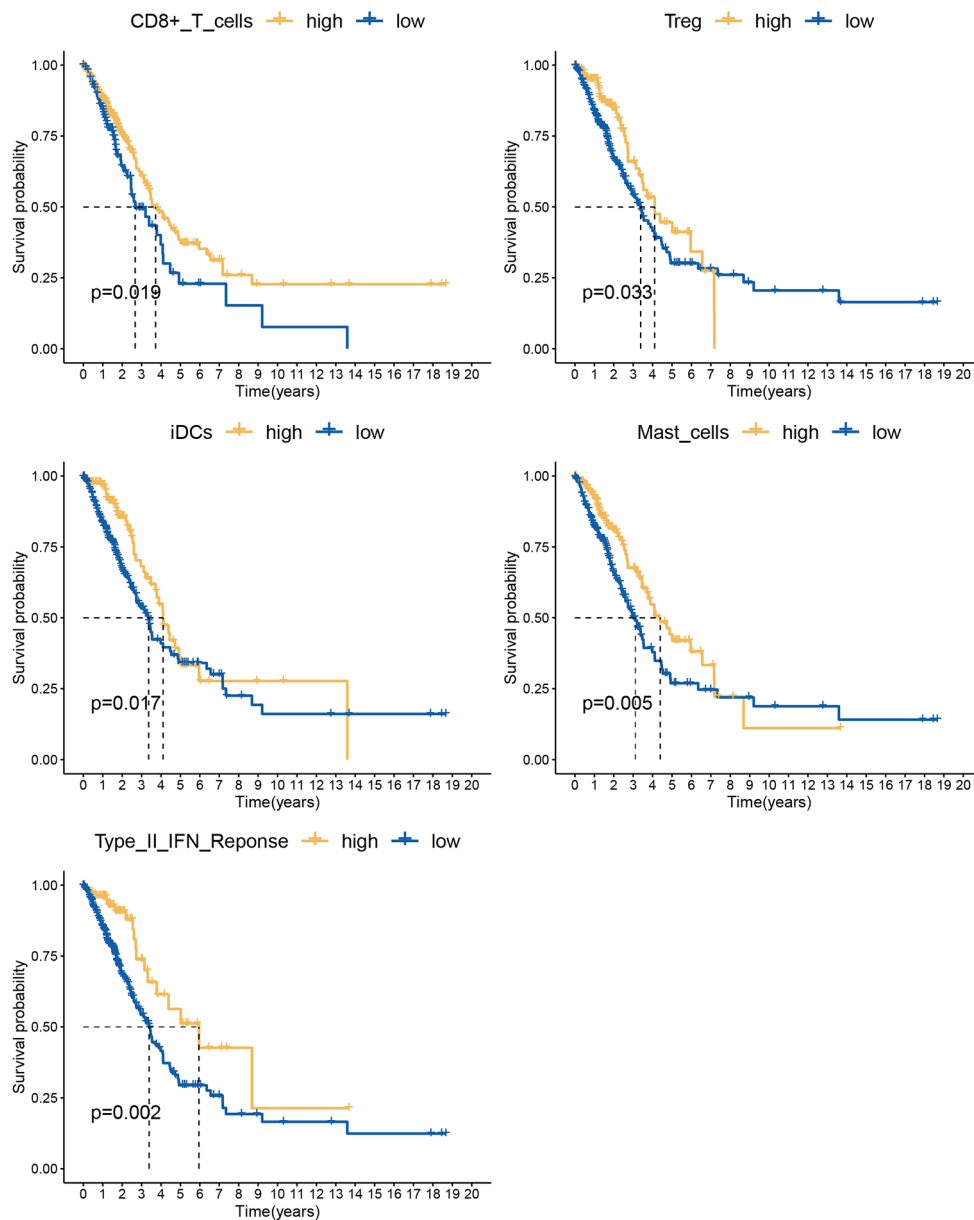


**Figure S5** Kaplan-Meier (K-M) survival analysis of immune-related functions with different expressions in 2 immune-related gene prognostic index (IRGPI) subgroups.

**Table S1** Kyoto Encyclopedia of Genes and Genomes (KEGG) pathways enriched in immune-related differentially expressed genes (DEGs)

ID	Description	GeneRatio	BgRatio	P value	P. adjust
hsa04060	Cytokine-cytokine receptor interaction	89/394	295/8091	2.42E-48	6.04E-46
hsa04061	Viral protein interaction with cytokine and cytokine receptor	37/394	100/8091	1.09E-23	1.36E-21
hsa04080	Neuroactive ligand-receptor interaction	54/394	341/8091	4.54E-15	3.76E-13
hsa04062	Chemokine signaling pathway	37/394	192/8091	2.86E-13	1.78E-11
hsa04630	JAK-STAT signaling pathway	32/394	162/8091	6.27E-12	3.12E-10
hsa04657	IL-17 signaling pathway	21/394	94/8091	2.88E-09	1.20E-07
hsa05323	Rheumatoid arthritis	19/394	93/8091	7.74E-08	2.75E-06
hsa04610	Complement and coagulation cascades	18/394	85/8091	9.58E-08	2.98E-06
hsa05417	Lipid and atherosclerosis	29/394	215/8091	5.02E-07	1.39E-05
hsa04064	NF-kappa B signaling pathway	18/394	104/8091	2.24E-06	5.58E-05
hsa05171	Coronavirus disease - COVID-19	28/394	232/8091	7.32E-06	0.000165615
hsa04380	Osteoclast differentiation	19/394	128/8091	1.22E-05	0.000253638
hsa04010	MAPK signaling pathway	32/394	294/8091	1.44E-05	0.000276659
hsa04668	TNF signaling pathway	17/394	112/8091	2.61E-05	0.000458062
hsa04621	NOD-like receptor signaling pathway	23/394	184/8091	2.76E-05	0.000458062
hsa04151	PI3K-Akt signaling pathway	35/394	354/8091	4.52E-05	0.00070387
hsa04014	Ras signaling pathway	26/394	232/8091	5.70E-05	0.000834168
hsa04360	Axon guidance	22/394	182/8091	6.89E-05	0.000953554
hsa04015	Rap1 signaling pathway	24/394	210/8091	8.05E-05	0.001054898
hsa04933	AGE-RAGE signaling pathway in diabetic complications	15/394	100/8091	8.92E-05	0.001110638
hsa05144	Malaria	10/394	50/8091	0.000119246	0.001355588
hsa05169	Epstein-Barr virus infection	23/394	202/8091	0.000119771	0.001355588
hsa05218	Melanoma	12/394	72/8091	0.000162323	0.001710843
hsa04350	TGF-beta signaling pathway	14/394	94/8091	0.000164901	0.001710843
hsa05133	Pertussis	12/394	76/8091	0.00027485	0.002737505
hsa05418	Fluid shear stress and atherosclerosis	17/394	139/8091	0.000397396	0.003667049
hsa01521	EGFR tyrosine kinase inhibitor resistance	12/394	79/8091	0.000397632	0.003667049
hsa04620	Toll-like receptor signaling pathway	14/394	104/8091	0.000482954	0.004294839
hsa04650	Natural killer cell mediated cytotoxicity	16/394	131/8091	0.000593909	0.005099427
hsa04614	Renin-angiotensin system	6/394	23/8091	0.000638591	0.005300309
hsa04024	cAMP signaling pathway	22/394	219/8091	0.000963935	0.007742578
hsa05167	Kaposi sarcoma-associated herpesvirus infection	20/394	194/8091	0.001180665	0.00918705
hsa04020	Calcium signaling pathway	23/394	240/8091	0.001411756	0.010652344
hsa04924	Renin secretion	10/394	69/8091	0.001729835	0.0126685
hsa05150	Staphylococcus aureus infection	12/394	96/8091	0.002302274	0.016286295
hsa04066	HIF-1 signaling pathway	13/394	109/8091	0.002354645	0.016286295
hsa04012	ErbB signaling pathway	11/394	85/8091	0.002627403	0.017681713
hsa04145	Phagosome	16/394	152/8091	0.002891555	0.018947294
hsa05219	Bladder cancer	7/394	41/8091	0.003289964	0.021005154
hsa05146	Amoebiasis	12/394	102/8091	0.003831773	0.023852788
hsa04625	C-type lectin receptor signaling pathway	12/394	104/8091	0.004493435	0.027289397
hsa04270	Vascular smooth muscle contraction	14/394	133/8091	0.005171768	0.030364107
hsa04928	Parathyroid hormone synthesis, secretion and action	12/394	106/8091	0.005243601	0.030364107
hsa05161	Hepatitis B	16/394	162/8091	0.005423714	0.030693293
hsa05226	Gastric cancer	15/394	149/8091	0.005864391	0.032402127
hsa05134	Legionellosis	8/394	57/8091	0.005985935	0.032402127
hsa05207	Chemical carcinogenesis - receptor activation	19/394	212/8091	0.007361743	0.039001573
hsa05162	Measles	14/394	139/8091	0.007608567	0.039469439
hsa05223	Non-small cell lung cancer	9/394	72/8091	0.007875125	0.040018494
hsa05143	African trypanosomiasis	6/394	37/8091	0.00827002	0.0411847
hsa04640	Hematopoietic cell lineage	11/394	99/8091	0.008465363	0.041330888
hsa04672	Intestinal immune network for IgA production	7/394	49/8091	0.009008454	0.043136636
hsa05340	Primary immunodeficiency	6/394	38/8091	0.009428056	0.044294073
hsa04926	Relaxin signaling pathway	13/394	129/8091	0.009882914	0.045571216
hsa05214	Glioma	9/394	75/8091	0.010229837	0.045687772
hsa05166	Human T-cell leukemia virus 1 infection	19/394	219/8091	0.010275161	0.045687772

**Table S2** Univariate and multivariate cox regression analysis of immune-related gene prognostic index (IRGPI) and clinical factors [age, gender, tumor (T), metastasis (M), and lymph node (N)]

Variables	Univariate Cox analysis				Multivariate Cox analysis			
	HR	HR95L	HR95H	p-value	HR	HR95L	HR95H	P value
Age	1.004	0.985	1.023	0.7	1.013	0.994	1.033	0.195
Gender	1.078	0.749	1.55	0.687	0.92	0.632	1.339	0.662
T	1.631	1.314	2.025	<0.001	1.241	0.978	1.576	0.075
M	1.78	0.976	3.242	0.06	1.717	0.917	3.214	0.091
N	1.794	1.462	2.201	<0.001	1.623	1.29	2.041	<0.001
IRGPI	1.098	1.068	1.129	<0.001	1.078	1.046	1.111	<0.001

**Table S3** Enriched pathways of immune-related differentially expressed genes (DEGs) in gene set enriched analysis (GSEA)

Description	setSize	enrichmentScore	NES	P value	P. adjust
SYSTEMIC_LUPUS_ERYTHEMATOSUS	108	-0.700210169	-2.236714273	1.00E-10	1.84E-08
CELL_CYCLE	121	0.574703456	2.19402952	4.03E-07	3.70E-05
FOCAL_ADHESION	177	0.490064778	1.970109543	3.85E-06	0.000235869
PROTEASOME	42	0.693281363	2.206226372	5.07E-05	0.002332459
ECM_RECEPTOR_INTERACTION	71	0.592614811	2.049230703	6.34E-05	0.002332829
PATHWAYS_IN_CANCER	288	0.371385484	1.543639028	0.000209649	0.006429231
REGULATION_OF_ACTIN_CYTOSKELETON	175	0.412060839	1.665088775	0.000944204	0.024819067
SMALL_CELL_LUNG_CANCER	79	0.510180417	1.823864275	0.001846318	0.042465306
DNA_REPLICATION	35	0.626889593	1.913638336	0.002571949	0.052582077
ASTHMA	20	-0.730757742	-1.762992145	0.002863025	0.052679661
PROXIMAL_TUBULE_BICARBONATE_RECLAMATION	19	-0.730437212	-1.727719996	0.003633549	0.06077936
PATHOGENIC_ESCHERICHIA_COLI_INFECTION	49	0.537429773	1.739493574	0.007362404	0.11289019
CYTOKINE_CYTOKINE_RECEPTOR_INTERACTION	193	0.359432836	1.455147952	0.008425906	0.117256955
P53_SIGNALING_PATHWAY	65	0.485176919	1.677399639	0.008943621	0.117256955
AXON_GUIDANCE	111	0.422190879	1.593107835	0.009985658	0.117256955
ADIPOCYTOKINE_SIGNALING_PATHWAY	59	-0.539358508	-1.574700597	0.010196257	0.117256955
SPLICEOSOME	125	0.40663282	1.564202992	0.011162246	0.117806307
NEUROACTIVE_LIGAND_RECEPTOR_INTERACTION	104	0.418019857	1.53885823	0.011559573	0.117806307
MELANOMA	54	0.481120743	1.605560995	0.012317879	0.117806307
HOMOLOGOUS_RECOMBINATION	26	0.625166147	1.835475822	0.012805033	0.117806307
OOCYTE_MEIOSIS	94	0.448305493	1.635022164	0.014123624	0.12374985
ALPHA_LINOLENIC_ACID_METABOLISM	15	-0.724497581	-1.634535987	0.015027571	0.125685142
ARRHYTHMOGENIC_RIGHT_VENTRICULAR_CARDIOMYOPATHY_ARVC	58	0.467601692	1.588697323	0.016563866	0.132510926
LINOLEIC_ACID_METABOLISM	17	-0.696664401	-1.597793528	0.018117388	0.138899978
ADHERENS_JUNCTION	69	0.441414319	1.540072764	0.024371308	0.179372827
PYRIMIDINE_METABOLISM	90	0.408774297	1.4872183	0.034616773	0.244980241
PPAR_SIGNALING_PATHWAY	55	-0.495789945	-1.422290124	0.03974359	0.262503671
PENTOSE_PHOSPHATE_PATHWAY	23	0.567769515	1.599608724	0.039946211	0.262503671
GLIOMA	58	0.42900605	1.45756693	0.044950999	0.281226567
FC_EPSILON_RI_SIGNALING_PATHWAY	69	-0.465332046	-1.390163002	0.045962733	0.281226567
RENAL_CELL_CARCINOMA	67	0.413786129	1.43035015	0.048223898	0.281226567